Regime-Dependent Nonstationary Relationship between the East Asian Winter Monsoon and North Pacific Oscillation

Gyundo Pak, Young-Hyang Park, Frédéric Vivier, Young-Oh Kwon, Kyung-Il Chang

Regime-Dependent Nonstationary Relationship between the East Asian Winter Monsoon and North Pacific Oscillation

GYUNDO PAK

LOCEAN/IPSL, Université Paris VI, and SEES, Seoul National University, Seoul, South Korea

YOUNG-HYANG PARK

LOCEAN/IPSL, Université Paris VI, and LOCEAN/DMPA, Muséum National d'Histoire Naturelle, Paris, France

FREDERIC VIVIER

LOCEAN/IPSL, Université Paris VI, Paris, France

YOUNG-OH KWON

Woods Hole Oceanographic Institution, Woods Hole, Massachusetts

KYUNG-IL CHANG

RIO/SEES, Seoul National University, Seoul, South Korea

(Manuscript received 20 August 2013, in final form 4 August 2014)

ABSTRACT

The East Asian winter monsoon (EAWM) and the North Pacific Oscillation (NPO) constitute two outstanding surface atmospheric circulation patterns affecting the winter sea surface temperature (SST) variability in the western North Pacific. The present analyses show the relationship between the EAWM and NPO and their impact on the SST are nonstationary and regime-dependent with a sudden change around 1988. These surface circulation patterns are tightly linked to the upper-level Ural and Kamchatka blockings, respectively. During the 1973–87 strong winter monsoon epoch, the EAWM and NPO were significantly correlated to each other, but their correlation practically vanishes during the 1988–2002 weak winter monsoon epoch. This nonstationary relationship is related to the pronounced decadal weakening of the Siberian high system over the Eurasian continent after the 1988 regime shift as well as the concomitant positive NPO-like dipole change and its eastward migration in tropospheric circulation over the North Pacific. There is a tight tropical–extratropical teleconnection in the western North Pacific in the strong monsoon epoch, which disappears in the weak monsoon epoch when there is a significant eastward shift of tropical influence and enhanced storm tracks into the eastern North Pacific. A tentative mechanism of the nonstationary relationship between the EAWM and NPO is proposed, stressing the pivotal role played in the above teleconnection by a decadal shift of the East Asian trough resulting from the abrupt decline of the EAWM since the late 1980s.

1. Introduction

The wintertime surface climate over the Far East and western North Pacific is under strong influence of the East Asian winter monsoon (EAWM), whose intensity is predominantly determined by that of the Siberian high (SH) (Gong et al. 2001; Park et al. 2012). The SH experienced a pronounced decadal weakening in the late 1980s (Nakamura et al. 2002; Panagiotopoulos et al. 2005), which resulted in changes in the relative importance between the EAWM and ocean dynamics in driving the regional sea surface temperature (SST) variability (Park et al. 2012). For more background knowledge on the EAWM, the reader is referred to some recent review papers (e.g., Chang et al. 2011; Huang et al. 2012).

Corresponding author address: Young-Hyang Park, LOCEAN/DMPA, Muséum National d'Histoire Naturelle, 43 Rue Cuvier, 75005 Paris, France.
E-mail: yhpark@mnhn.fr

DOI: 10.1175/JCLI-D-13-00500.1

In addition to the EAWM, the North Pacific Oscillation (NPO), a surface expression of the west Pacific (WP) teleconnection pattern (Wallace and Gutzler 1981), is also known to influence the winter SST variability in the western North Pacific. For example, Yeh and Kim (2010) claimed that the long-term winter SST variability in the Yellow/East China Sea is best attributable to the NPO. However, this is in contrast with Park et al. (2012) who showed that winter SST anomalies averaged over the East Asian marginal seas are much better correlated with the EAWM than with the WP, although these indices are significantly correlated to each other.

A precise knowledge of the interrelationship among the EAWM, NPO/WP, and winter SST as well as the relative importance of each atmospheric circulation pattern for the spatial distribution of SST variability, together with their time evolutions in different climate regimes, is required for better understanding the atmosphere–ocean interaction in the western North Pacific. The latter topic has recently attracted an increasing interest especially in the subpolar frontal regions of the western North Pacific, such as in the Kuroshio–Oyashio Extension region (Kwon et al. 2010; Frankignoul et al. 2011) and the Japan/East Sea (JES) (Hirose et al. 2009; Yamamoto and Hirose 2011). We will show here that the nonstationary regime-dependent relationship between the EAWM and NPO is closely linked with the upper-level blocking activities over the Ural and Kamchatka regions, of which the potential underlying dynamics are analyzed in terms of regime-dependent changes in storm tracks, tropical influence, and stationary wave activity flux.

2. Data and atmospheric circulation indices

Two principal datasets used here for surface climate include monthly SST and sea level pressure (SLP). The Hadley Centre Sea Ice and Sea Surface Temperature dataset (HadISST; Rayner et al. 2003; available online at http://www.metoffice.gov.uk/hadobs/hadisst/) is used for the SST. For SLP, we used the so-called Trenberth SLP data (Trenberth and Paolino 1980) (http://rda.ucar.edu/datasets/ds010.1/). In addition, we used the daily fields of geopotential height at 300 hPa (Z300) and 500 hPa (Z500) from the National Centers for Environmental Prediction–National Center for Atmospheric Research (NCEP–NCAR) Reanalysis-1 (Kalnay et al. 1996) (http://www.esrl.noaa.gov/psd/data/gridded/data.ncep.reanalysis.html) to investigate upper-level blocking events and storm-track activity. We also used other supplementary monthly-mean atmospheric data from the NCEP–NCAR, which will be noted in appropriate places.

The SH index is defined as the area-mean SLP anomalies over the SH center (45°–55°N, 85°–105°E) and the EAWM index as the difference between the SH index and area-mean SLP anomalies in the southeastern JES (35°–40°N, 135°–140°E) following Park et al. (2012). The NPO index is defined as the difference of SLP anomalies between two centers of action (65°N, 170°E and 25°N, 165°E) following Wallace and Gutzler (1981). Note that this NPO index has no significant difference ($r = 0.82$) from that suggested by Linkin and Nigam (2008), who used the second principal component of SLP anomalies in the North Pacific north of 20°N. The Aleutian low (AL) index is used as a synonym of the North Pacific index defined as the area-mean SLP anomalies over the area (30°–65°N, 160°E–140°W) following Trenberth and Hurrell (1994). The WP index, Arctic Oscillation (AO) index, and Pacific–North American (PNA) teleconnection pattern index are taken from the National Oceanic and Atmospheric Administration (NOAA)/Climate Prediction Center website (http://www.cpc.ncep.noaa.gov/data/teledoc/telecontents.shtml). The El Niño–Southern Oscillation (ENSO) index we used is the multivariate ENSO index (MEI) from the NOAA/Earth System Research Laboratory website (http://www.esrl.noaa.gov/psd/enso/mei/).

In this study, we focus on the climate variability during boreal winter—December through February (DJF) for atmospheric variables and January through March (JFM) for SST, if not otherwise stated—for 48 winters between 1965 and 2012. Our convention of year corresponds to that containing January.

3. Regime-dependent relationship between EAWM and NPO

a. Regime shifts and corresponding relationship between EAWM and NPO

To objectively determine the exact regime shifts that occurred during the past several decades in the North Pacific, we applied the sequential *t*-test analysis of regime shift (Rodionov 2004) using the code from NOAA (http://www.beringclimate.noaa.gov/regimes/; see Fig. 1 caption for the parameters used for the analysis). This method uses a sequential data processing technique so that it exhibits a limitation of the solution being less reliable if a regime shift is too close to the end of a time series, as commonly encountered by other regime shift detection methods. See Rodionov (2004) for more details.

Figure 1a shows the results for different indices discussed here together with the corresponding normalized cumulative sums. The cumulative sum has been known to be very useful for a visual validation of regime shifts (Tian et al. 2008), and we observe in fact that all detected regime shifts coincide within ±1 yr with the extremes of the cumulative sum. A major regime shift in the four dominant climate indices of the western North

Pacific (EAWM, NPO, SH, and WP) occurred between 1987 and 1989. For the sake of simplicity in the subsequent analyses, we take the year 1988 as the representative regime shift common to these four indices. The 1988 regime shift detected in Fig. 1a is consistent with Wang et al. (2009). Furthermore, there is evidence of the latest regime shift around 2010 for all four indices, although it should be interpreted with caution because of the limited data length after 2010. Accordingly, we define two distinct winter climate regimes in the western North Pacific: a strong monsoon regime during 1965–87 and a weak monsoon regime during 1988–2010.

Supplementary analysis with the dominant teleconnection patterns in the eastern North Pacific such as the AL index and the PNA index reveals the well-known 1976/77 regime shift (see Fig. 1a), in good agreement with Hare and Mantua (2000). These authors and Yeh et al. (2011) reported another major regime shift in 1988/89 in the North Pacific SST. We note here that the latter regime shift around 1988 is found in the dominant climate indices in the western North Pacific while that around 1977 is found in the eastern North Pacific. Although Wang et al. (2007) showed that the typical periodicity of the NPO changed from 3 yr before 1976 to 5–6 yr afterward, we do not find any clear evidence of its regime shift around 1976 (see Fig. 1). Note that the 1988 regime shift is also observed in the AO index and no regime shift is detected in the ENSO index. Finally, there is evidence of the latest regime shift around 2010 for all indices but one (PNA).

The 11-yr running correlation coefficient between the EAWM and NPO indicates that the two indices were not always well correlated with each other (Fig. 1b) but their relationship reveals pronounced low-frequency variations, suggesting in particular insignificant correlations before the early 1970s, largely consistent with Wang et al. (2007), and in the 1990s. The EAWM–NPO correlation as well as the EAWM intensity recovered gradually since the early 2000s, the latter being also consistent with Wang and Chen (2014a). Similar results are obtained with varying window size between 9 and 15 yr. All correlation coefficients shown in this paper have been calculated with detrended data for each subperiod. It is remarkable that the transition from significant to insignificant correlations occurred very close to the 1988 regime shift. As we are interested here in the nonstationary relationship between the EAWM and NPO, we select two contrasting 15-yr-long epochs before and after the 1988 regime shift, with a significant correlation versus an insignificant one as the strong monsoon–high correlation (SM–HC) epoch (1973–87) and the weak monsoon–low correlation (WM–LC) epoch (1988–2002). If not explicitly stated otherwise, the regime-dependent

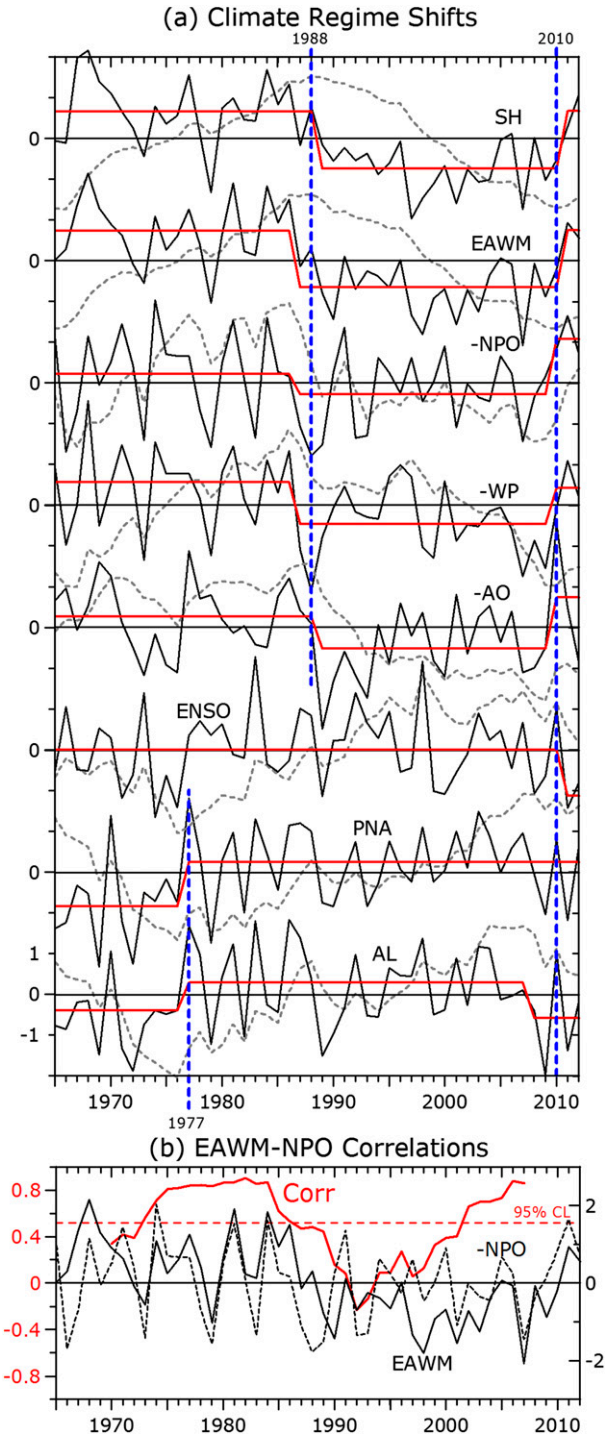

FIG. 1. (a) Climate regime shift determination (red) from normalized climate indices (black) based on Rodionov (2004), together with normalized cumulative sums (dotted gray). For the regime shift determination, the following parameters are used: cutoff length in yr = 10; probability level = 0.15; and Huber weight (or outlier) in standard deviation = 1.5. (b) 11-yr running correlation coefficient (red) between the EAWM (solid black) and negative NPO (dotted black) indices. The horizontal dotted red line indicates the 95% confidence level, with a constant degree of freedom equal to 9.

comparison described hereafter should be understood as using the above two epochs, which will be clearer in the text. Indeed, during the SM–HC epoch, the EAWM index is practically indistinguishable from the NPO index ($r = -0.89$), while the two indices became nearly independent ($r = -0.11$) during the WM–LC epoch (Table 1). The SH–NPO pair shows similar results, albeit with somewhat weaker correlations compared to the EAWM–NPO pair. The WP is generally better correlated than NPO with both the EAWM and SH.

b. *Regime-dependent impact of EAWM and NPO on the SST*

During the entire analysis period (1965–2012), the EAWM and NPO were equally well projected onto the regional SST variability (Figs. 2a,d). However, a close inspection shows a subtle difference; the EAWM is slightly more influential in the East Asian marginal seas, whereas the NPO is a little better projected in the Kuroshio recirculation region and in the subpolar gyre region southeast of Kamchatka. This can be best seen in the difference map of squared correlations (Fig. 2g). The magnitude of the SST anomaly associated with the EAWM and NPO in the western North Pacific is typically 0.4°–0.7°C in the marginal seas and 0.2°–0.3°C in the open ocean gyre regions, as revealed from a regression (not shown).

The SST projection of the EAWM and NPO during the SM–HC epoch (1973–87) reveals nearly the same pattern but with somewhat overall higher correlations compared to that of the entire period (Figs. 2b,e,h). The most striking feature during the WM–LC epoch (1988–2002) is that the impact of the EAWM was weakened and shrunk remarkably into a limited area in the East China Sea and southern JES (Fig. 2c). The impact of the NPO was also much weakened especially in the Kuroshio recirculation region but slightly strengthened in the subpolar gyre region (Figs. 2f,i), showing a clearer geographical separation from the EAWM impact, consistent with their insignificant correlation during the WM–LC epoch (see Table 1).

c. *Regime-dependent changes of SH and atmospheric circulation*

As the EAWM index is very highly correlated ($r =$ 0.77–0.95) with the SH index (Park et al. 2012; see also Table 1), we will analyze below the regime-dependent influence of the SH (as a proxy of the EAWM) in relation to that of the NPO. The SH center is located to the southwest of Baikal Lake, with its easternmost extension over northeastern Siberia reaching as far east as the Bering Strait (Fig. 3a). The subpolar center of the NPO is located at the northwestern border of the AL system, touching the northeastern "tail" of the SH system, while

TABLE 1. Correlation coefficients between pairs of climate indices for 1965–2012, with significant correlations at the 95% confidence level marked in boldface. Shown in parentheses are the correlation coefficients for two epochs: SM–HC (1973–87) and WM–LC (1988–2002).

Indices	EAWM	NPO	WP	AO	ENSO	PNA	AL
SH	**0.91 (0.93, 0.77)**	**−0.40 (−0.81**, 0.18)	**−0.45 (−0.85**, 0.09)	−0.16 (−0.10, 0.02)	−0.28 (−0.42, −0.14)	0.19 (**0.52**, 0.13)	0.10 (0.35, −0.13)
EAWM		**−0.53 (−0.89**, −0.11)	**−0.57 (−0.92**, −0.15)	**−0.29** (−0.09, −0.13)	**−0.32 (−0.53**, −0.18)	0.14 (0.44, 0.02)	0.12 (0.33, −0.09)
NPO			**0.80 (0.92, 0.61)**	0.14 (0.04, 0.00)	**0.53 (0.76**, 0.14)	0.12 (−0.14, 0.33)	0.13 (−0.01, 0.28)
WP				0.10 (0.08, −0.14)	**0.45 (0.68**, 0.14)	−0.04 (−0.26, 0.31)	−0.12 (−0.22, 0.04)
AO					−0.18 (−0.00, −0.33)	−0.24 (−0.24, **−0.59**)	**−0.38** (−0.34, **−0.63**)
ENSO						**0.44** (0.36, **0.60**)	**0.51** (0.37, **0.72**)
PNA							**0.92 (0.93, 0.86**)

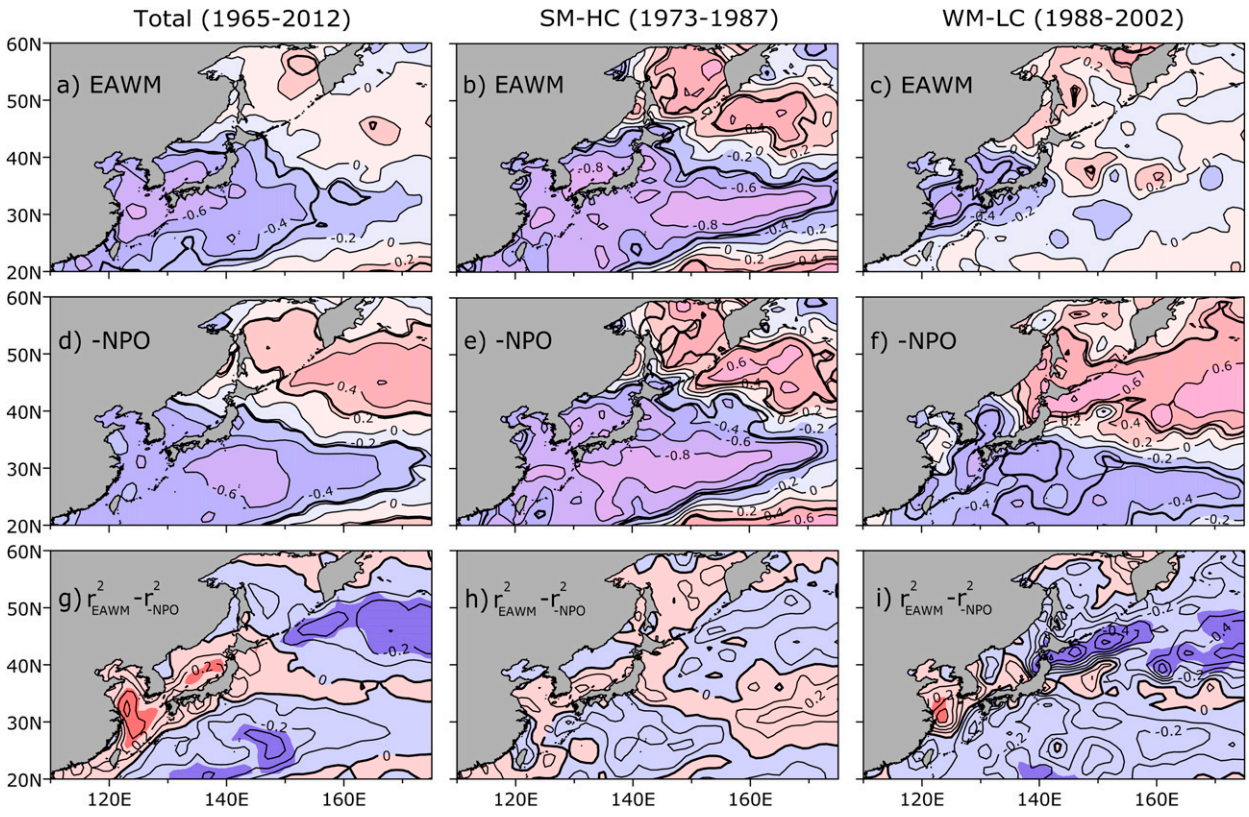

FIG. 2. Correlation coefficients of JFM SST anomalies with (a)–(c) the EAWM and (d)–(f) the negative NPO for three different periods, with significant correlations at the 95% confidence level marked with the thicker curves. The effective degrees of freedom (e.g., Emery and Thomson 1997) are estimated at each grid point. (g)–(i) Difference map of squared correlations (red color for the EAWM dominant regions), with a significant difference (at 90%) shaded with a stronger tone.

its subtropical center is found near the Kuroshio recirculation gyre. At the 500 hPa, the SH center and the subpolar center of the NPO are found respectively upstream and downstream of the well-developed East Asian trough (Fig. 4a).

During the SM–HC epoch (1973–87), the correlation map of SLP with the SH index (Fig. 5a) shows that the area with significant correlations extended far eastward, revealing a high and same sign (opposite sign) correlation with the subpolar (subtropical) center of the NPO, showing a tight linkage between the two circulation patterns. This tight connection can be verified when correlations are calculated in reference to the NPO index (Fig. 5c). During the WM–LC epoch (1988–2002), on the contrary, the area with significant correlations with the SH index shrank radically around the SH center, thus disconnected completely from the two centers of the NPO (Fig. 5b). Similar comments on such a disconnection can be made in reference to the NPO index (Fig. 5d).

Figures 3b and 4b suggest that the change in the EAWM–NPO relationship between the two epochs is associated with the hemispheric (planetary wave–like) changes in epoch-mean SLP and Z500 anomalies, which are superimposed on the overall opposite changes between the polar and middle latitudes. The latter feature in Fig. 3b resembles the spatial pattern of SLP anomalies during a positive phase of the AO, which has intensified substantially after the 1988 regime shift (e.g., Yeh et al. 2011, among others). Most noticeable among the mid-latitude changes relevant to our study is the abnormal weakening of SLP over the Eurasian continent, especially around the SH center during the WM–LC epoch, which is paired with a concomitant weakening of the southeastern part of the AL system over the eastern North Pacific, consistent with Yeh et al. (2011). These surface circulation changes between the two epochs over the Eurasian continent and North Pacific are more clearly visible in the upper-level circulation represented by changes in $Z500$ (Fig. 4b), with a pair of northwest–southeast oriented opposite centers of action over Siberia and an another pair of north–south oriented opposite centers at about 170°W in the North Pacific. We will show below that these are well linked to upper-level blocking features.

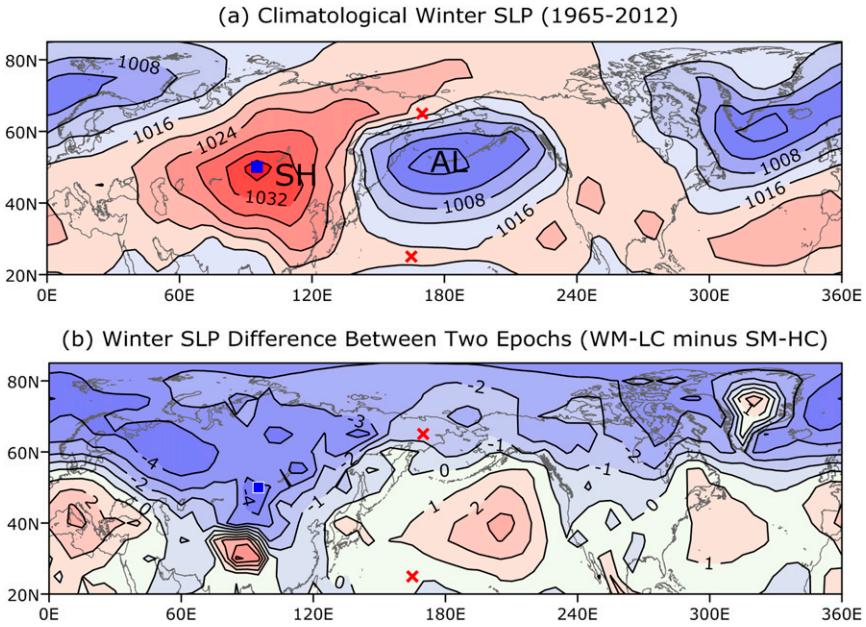

FIG. 3. (a) Climatological winter-mean SLP (in hPa) in the Northern Hemisphere north of 20°N during 1965–2012. The SH center (blue square) and the two centers of the NPO (red crosses) are indicated. (b) Winter SLP difference between two contrasting epochs: WM–LC (1988–2002) minus SM–HC (1973–87).

4. Ural and Kamchatka blockings controlling SH/EAWM and NPO

Takaya and Nakamura (2005a) pointed out that intraseasonal amplification of the SH can be caused by upper-level blocking over Siberia west of the climatological upper-level trough over the Far East, called ''wave train'' (Atlantic origin) type, which occurs in turn by amplification of quasi-stationary Rossby wave train coming from the Euro–Atlantic sector. Takaya and

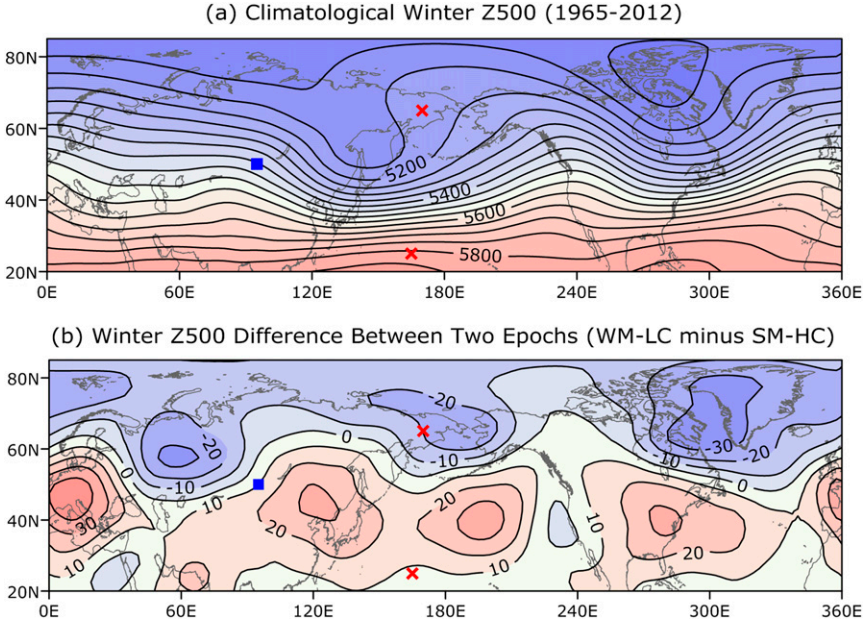

FIG. 4. (a) Climatological winter-mean $Z500$ (in m) in the Northern Hemisphere north of 20°N during 1965–2012. (b) Winter $Z500$ difference between two contrasting epochs: WM–LC (1988–2002) minus SM–HC (1973–87).

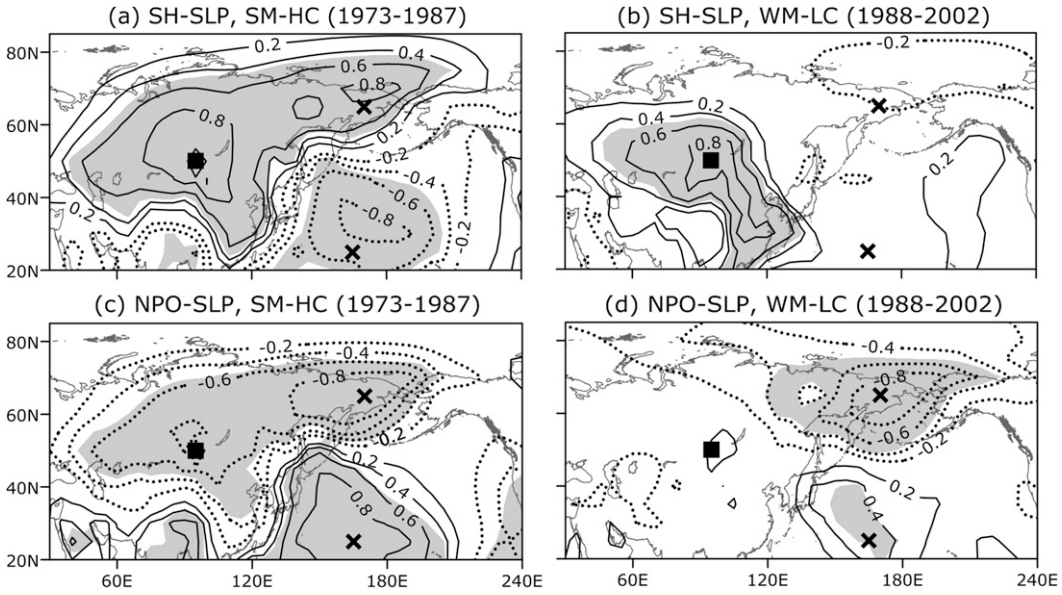

FIG. 5. (a),(b) Correlation maps of SLP anomalies with the SH index for the SM–HC epoch (1973–87) and the WM–LC epoch (1988–2002), respectively. (c),(d) As in (a),(b), but for the NPO index. The areas with significant correlations at the 95% confidence level are shaded.

Nakamura (2005b) further suggested that the blocking to the east of the trough, called "Pacific origin" type, also affects the SH especially in the northeastern Siberia region. For the commodity of naming according to the representative landmark in the vicinity of the above two blockings, we will refer to them in the present paper as "Ural blocking" and "Kamchatka blocking," respectively.

A blocking index (BI) is calculated as the normalized projection of monthly Z500 anomaly patterns onto the composite blocking pattern (Wang et al. 2010) as

$$\mathrm{BI} = \frac{\langle \Delta Z_b, \Delta Z_m \rangle}{\langle \Delta Z_b, \Delta Z_b \rangle},$$

where ΔZ_b is the winter composite of daily $Z500$ anomaly fields corresponding to the days of blocking events based on Barriopedro et al.'s (2006) criteria applied over a selected blocking sector, ΔZ_m is the monthly-mean $Z500$ anomaly field, and the brackets denote an inner product over a given projection area in each winter. We defined the Ural (Kamchatka) blocking sector as 40°–80°E (140°E–180°) with a reference latitude of 60°N.

Figures 6a and 6c represent the composited blocking pattern ΔZ_b during 1965–2012 over the projection area for the Ural blocking (30°–85°N, 30°W–150°E) and Kamchatka blocking (30°–85°N, 70°E–110°W), respectively. The Ural blocking (at 500 hPa) is characterized by a well-defined blocking high over the Ural Mountains, which is associated with a downstream low over the surface high SH center (see also Figs. 3b and 4b), while the Kamchatka blocking reveals a north–south dipole pattern, very similar to that of the WP/NPO (Wallace and Gutzler 1981).

Consistent with Wang et al. (2010), the Ural blocking index is highly correlated with the SH index ($r = 0.70$; Fig. 6b). As expected, it is also highly correlated with the EAWM index ($r = 0.68$). Takaya and Nakamura (2005a) showed that the SH amplification is achieved through vertical coupling in which upper-level potential vorticity anomalies associated with the wave train induce anomalous cold advection in the downstream side of a blocking ridge, reinforcing the preexistent cold anticyclonic anomalies at the surface. The Kamchatka blocking is very tightly linked to the NPO ($r = -0.82$; Fig. 6d), which is, to our knowledge, first to be reported. Furthermore, the Kamchatka blocking can be interpreted as the WP itself because their correlation reaches as much as -0.92, in addition to the very similar dipole pattern mentioned above. During the SM–HC epoch, the Ural and Kamchatka blocking indices were highly correlated ($r = 0.76$) to each other, while their correlation practically vanished ($r = 0.18$) during the WM–LC epoch, in good agreement with the results from the SLP data (see Fig. 5).

5. Regime-dependent dynamics associated with the nonstationary relationship

a. *Potential factors affecting the wintertime stationary waves: A review*

The mechanism responsible for the nonstationary relationship between the EAWM and NPO has not been

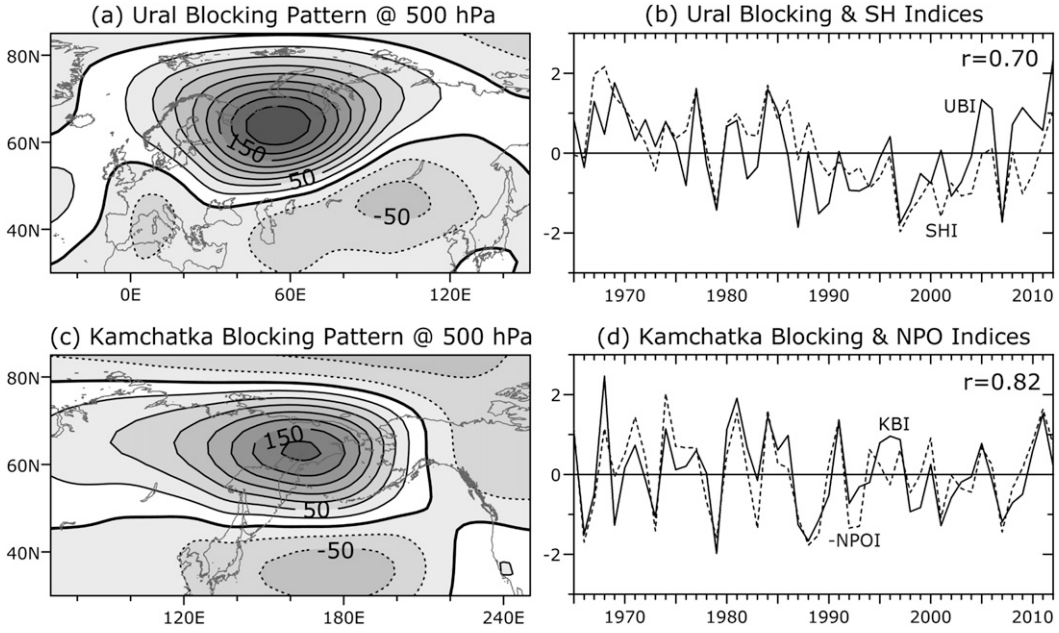

FIG. 6. Blocking pattern ΔZ_b (in m) over the projection area for (a) the Ural blocking and (c) the Kamchatka blocking. Comparison between (b) the Ural blocking index (UBI; solid) and SH index (SHI; dotted) and (d) the Kamchatka blocking index (KBI; solid) and negative NPO index (NPOI; dotted).

addressed previously but constitutes the most challenging issue. To get some useful information on it from the observational data, it is necessary to document first the possible causes of the 1988 regime shift of the individual index. For the EAWM case, several hypotheses have been advanced for the recent decline of the SH/EAWM since the late 1980s: reduction of continent blockings over the Ural Mountains region (Wang et al. 2010) associated with changing quasi-stationary Rossby wave train coming from the Euro–Atlantic sector (Takaya and Nakamura 2005a); global warming (Hori and Ueda 2006); and reduction of Arctic sea ice cover and the associated Arctic warming (Li et al. 2014). In contrast, few studies have addressed the causes of the 1988 regime shift of the NPO. In an effort to find some observational evidence of dynamics underlying the regime shift in question, major potential factors affecting the wintertime stationary waves are reviewed below.

The NPO/WP and AL/PNA are two representative wintertime stationary wave patterns in the North Pacific, each concentrated in the western and eastern basins, respectively. According to the theoretical and modeling study of Held et al. (2002), there are three forcing factors affecting the northern winter stationary waves: namely, orography, diabatic heating, and momentum transients. The Tibetan Plateau exerts the most important orographic forcing in the EAWM sector, generating wave trains, with a part refracting strongly into the tropics and a part propagating poleward before arcing toward the tropics. The most conspicuous anomaly center in the midtropospheric circulation associated with the Tibetan orographic forcing may be a well-defined negative (cyclonic) center located just north of the Korean Peninsula (45°N, 125°E), which is paired with a tropical positive (anticyclonic) center (20°N, 130°E) (Fig. 3 of Held et al. 2002). As the linear response to orography is approximately proportional to the strength of the low-level mean winds (Held and Ting 1990), the former cyclonic center can be interpreted as the manifestation of the deepened East Asian trough (see Fig. 4a), the intensity of which is well correlated with that of the EAWM (Wang and Chen 2010).

There are two major heating sources in the North Pacific: tropical heating (south of 25°N) and extratropical heating (north of 25°N) mostly centered in the Kuroshio–Oyashio Extension region (Fig. 8 of Held et al. 2002). Tropical heating involves deep vertical motion and upper-level divergence that generates poleward-propagating Rossby waves and presents two major sources: one in the western tropical warm pool region near the Philippines and the other in the central equatorial region. The western tropical heating source seems to generate the NPO-like teleconnection pattern, with wave train–like upper-level circulation anomalies developed along the east coast of East Asia, with a tropical anticyclonic center just north of the Philippines and a cyclonic center in the JES (Fig. 16d of Jin and Hoskins 1995). These show the same signs and are located nearly

in the same area as the Tibetan wave train. In addition, a high-latitude anticyclonic center is found just west of Kamchatka. The central equatorial heating source, which should be most effective during the El Niño (warm) phase of ENSO, displays a PNA-like wave train in the eastern basin having a roughly opposite phase compared to the western NPO-like wave train, with a cyclonic center near Hawaii, an anticyclonic center in the Gulf of Alaska, and a cyclonic center over western Canada (Fig. 16a of Jin and Hoskins 1995).

Storm tracks are thought to play a significant role in the extratropical wave train forced by El Niño and the direct effect of tropical forcing should be large in the jet exit region (eastern North Pacific basin), where the storm-track eddy momentum fluxes are concentrated (Held et al. 2002). Storm-track variability is believed to be composed of all of above factors, as part of it is internal atmospheric noise, part of it is tropically driven, and part of it is impacted by ocean–atmosphere coupling (Kwon et al. 2010). So it can be used as a diagnostic to show which influence dominates.

Following the above short review, we will explore in the following subsections supplementary observational evidence associated with different dynamics underlying changes for two periods before and after the regime shift, which is a prerequisite to better understand the mechanism of the regime shift itself. A tentative synthesis of the latter mechanism is given at the end of section 5d.

b. *Evolution of storm tracks across the regime shift*

Figure 7 shows the spatial distribution of storm-track activity measured by 2–6-day bandpass filtered $Z300$ variance for the SM–HC and WM–LC periods as well as their difference (WM–LC minus SM–HC). For both periods, zonally elongated storm tracks are developed along ~40°N, with their peaks being located in the central basin close to the date line. Compared to the SM–HC period, the storm tracks during the WM–LC period were strengthened significantly and extended far eastward into the eastern basin, whereas a noticeable weakening is observed at higher latitudes at the northeastern corner of Siberia (Fig. 7c).

Figure 8 shows two leading empirical orthogonal functions (EOFs) and corresponding principal components (PCs) of storm tracks for the entire analysis period (1965–2012). The EOF1 shows a zonally elongated monopole developed along 40°N in the central basin, a feature very similar to the raw storm-track pattern (Fig. 7), whereas the EOF2 reveals a north–south dipole pattern straddling a nodal line at 40°N, mostly confined within the eastern basin east of the date line. Interestingly, the PC1 (Fig. 8b) reveals a clear regime shift

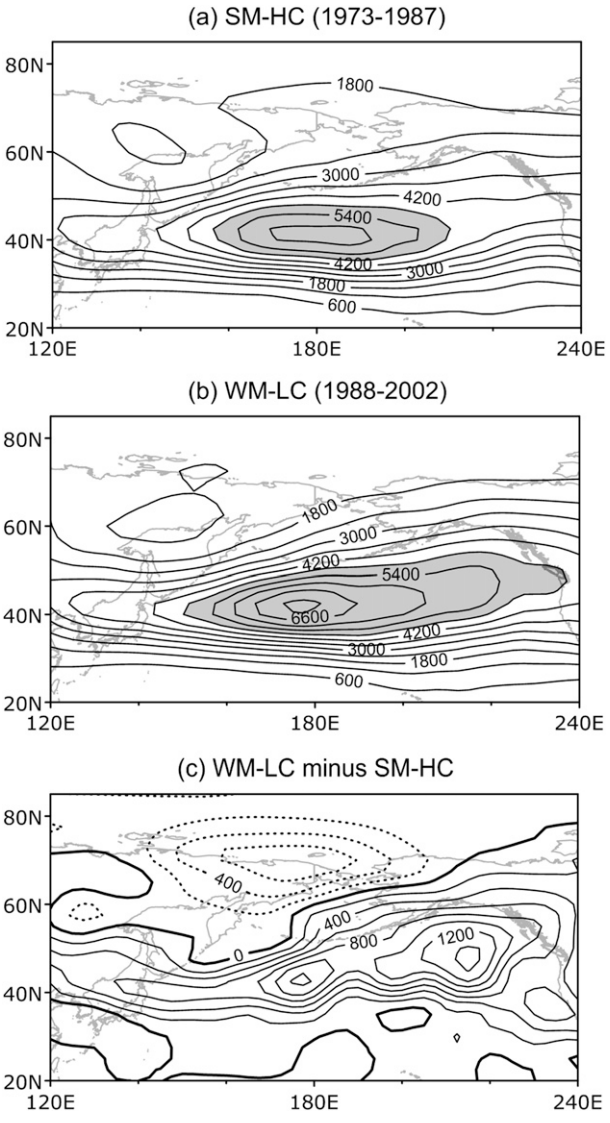

FIG. 7. Time-mean storm-track intensity measured by 2–6-day bandpass filtered $Z300$ variance for the (a) SM–HC and (b) WM–LC periods. Contour interval is 600 m^2 and the area of intensity over 4800 m^2 is darkly shaded. (c) Difference in intensity between the two periods, with the contour interval of 200 m^2 and negative anomalies shown by dotted lines.

around 1987, much the same as the NPO shown in Fig. 1, which can be easily verified by the corresponding SLP regression (not shown). On the other hand, the PC2 (Fig. 8d), which is associated with the AL (or PNA)-like SLP pattern, shows dual regime shifts in 1977 and 1987, although such is somewhat at odd with the unique regime shift of AL and PNA in 1977 seen in Fig. 1.

When the SLP is regressed on the storm-track PC1 separately for the SM–HC and WM–LC (Figs. 9a,c), the NPO-like pattern during the latter period shifts eastward by up to 20° in longitude compared to the former

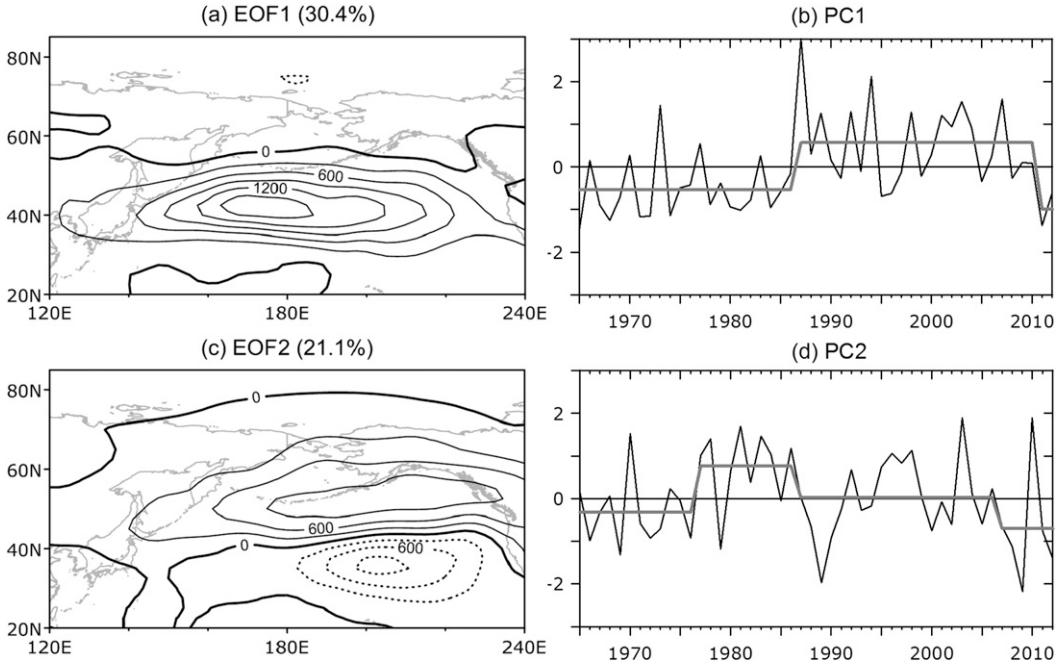

FIG. 8. Storm-track EOF and corresponding PC for the (a),(b) first mode and (c),(d) second mode. Contour interval is 300 m^2 and negative values are dotted in (a),(c). Regime shift determination is shown by thick lines in (b),(d).

period. Also, the northwest–southeast oriented nodal line during the SM–HC becomes nearly zonal because of its northward shift in the eastern basin during the WM–LC. Note that the SLP regression pattern in SM–HC is very close to the NPO defined by Wallace and Gutzler (1981), while the one in the WM–LC is similar to the EOF2 pattern shown by Linkin and Nigam (2008) and Ceballos et al. (2009). A similar eastward shift is also observed in the EOF2 of *Z*500 anomalies in the latter period (cf. Figs. 9b,d).

One is tempted to interpret Fig. 9, which shows storm-track-related circulation patterns, as the eastward-shifting NPO pattern because of its similar projection onto the latter pattern. However, the NPO as defined in the present paper according to Wallace and Gutzler (1981) does not show any eastward shift (see Figs. 5c,d). On the other hand, Zhu and Sun (1999) showed previously that ENSO exerts an important influence on the maintenance and development of the North Pacific winter storm track. We will test below this possibility and show in effect that the observed eastward shift of intensified storm track and its related tropospheric circulation pattern during the WM–LC is consistent with a significant eastward shift of the ENSO influence toward the eastern basin.

c. *Evolution of tropical influence across the regime shift*

To document the regime-dependent tropical–extratropical connection, we present in Fig. 10 lag correlations of the winter (DJF)-mean EAWM and NPO indices relative to the lagged 3-month-mean MEI (representing the seasonal ENSO forcing) for two contrasting periods before and after the regime shift. This is done by successively sliding the MEI time series by 1 month over a total lag range of ±2 yr such that a positive (negative) lag indicating the EAWM/NPO (ENSO) leading. During the SM–HC, the most significant correlation is observed at the zero lag for both the EAWM and NPO, although the NPO shows a much tighter connection with ENSO (r = 0.76: significant at more than the 99% level) compared to a moderate EAWM–MEI relationship (r = 0.53: significant at the 95% level but not exceeding the 99% level). The observed rapid decrease in correlation with increasing lag in either positive or negative direction with an insignificant correlation at a few months of lag may attest the simultaneous EAWM–ENSO and NPO–ENSO connections. Furthermore, as the EAWM and NPO are highly correlated during the SM–HC as already shown, Fig. 10a may suggest a possibility of the simultaneous EAWM–ENSO–NPO triple connection in this period.

In great contrast to this, in the WM–LC no significant correlation between the ENSO and EAWM or NPO appears at any lag, except for one exception of a moderate correlation (r = 0.50) with the EAWM at a lag of −1 yr, which indicates that the preceding winter ENSO affects somewhat the contemporaneous EAWM. However, such is not observed in the SM–HC, during which

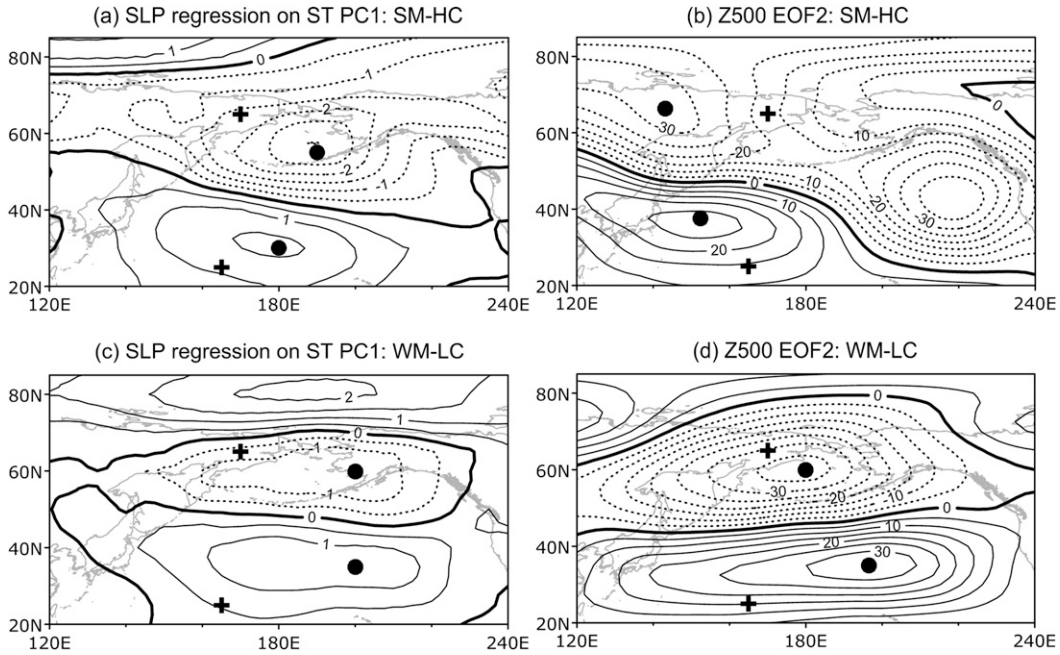

FIG. 9. Regression maps of anomalous winter SLP on the storm-track PC1 for the (a) SM–HC and (c) WM–LC periods. EOF2 of anomalous winter *Z*500 for the (b) SM–HC and (d) WM–LC periods. Contour intervals are 0.5 hPa for (a),(c) and 5 m for (b),(d). Crosses represent the two centers of action of NPO according to Wallace and Gutzler (1981), whereas black circles are those from the mapped patterns.

there is evidence that the contemporaneous EAWM rather affects ENSO marginally ($r = 0.45$) in two years. On the other hand, except for the highest correlation centered at the zero lag in the SM–HC, no significant lagged correlation is observed between the NPO and ENSO for both periods. Though not significant at the 95% level, the strongest correlation ($r \sim -0.4$) between the NPO and ENSO during the WM–LC occurs when the NPO leads ENSO by about 1 yr, which might support the seasonal footprinting mechanism of Vimont et al. (2003). However, such is not observed for the SM–LC, during which the 1-yr lag correlation between the two indices is close to zero, suggesting that the NPO feedback on ENSO is not a robust feature in our analysis. We will focus below on the simultaneous relationship between ENSO and both the NPO and EAWM.

Figure 11 illustrates the maps of contemporaneous correlation of winter *Z*300, *Z*500, and SLP anomaly fields relative to the MEI separately for the SM–HC and WM–LC. For these two periods, both common and contrasting features appear. As expected, the most widespread and significant positive correlation with ENSO is found in the tropics south of 20°N regardless of the tropospheric levels and periods, except for the SLP in the eastern tropics, where the sign is reversed, in line with the classical ENSO definition. The most remarkable difference between the two periods is that in the SM–HC the significant tropical influence extends much farther northward up to 40°N in the western boundary region (including the Kuroshio recirculation region and the JES) compared to its near-zonal poleward limit at ~20°N during the WM–LC. This is accompanied with a maximum negative correlation near the northern NPO center in the former period (Figs. 11a,c), which is in great contrast to its absence in the latter period (Figs. 11b,d). On the other hand, another negative maximum centered at (40°N, 140°W) in the eastern basin is paired with a positive pole found over northeast Canada, which is a common feature to both periods but with a slight intensification in the latter period. This feature is most evident in the *Z*300 and *Z*500 maps and resembles much the PNA teleconnection pattern.

Concerning the SLP maps, we remark that in the SM–HC (Fig. 11e) both the northern and southern NPO centers are well correlated with ENSO, with a significant negative correlation at the northern center extending westward to the SH center. This is consistent with the observed significant triple correlations among the EAWM, NPO, and ENSO during the SM–HC (see Table 1). In contrast, this triple connection vanishes in the WM–LC (Fig. 11f) during which the ENSO influence disappears at both the northern NPO center and the SH center, although a significant but somewhat weakened ENSO influence is still visible at the southern NPO center.

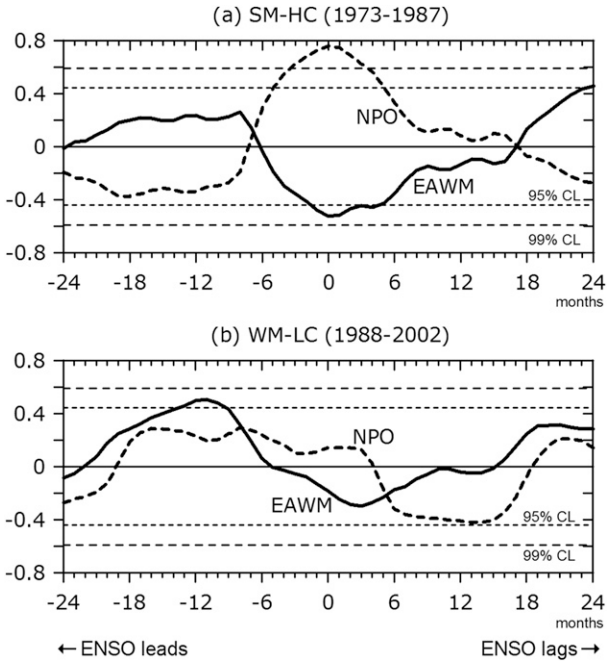

FIG. 10. Lag correlations of the EAWM index (solid line) and NPO index (thick dotted line) with lagged ENSO index (MEI) for the (a) SM–HC and (b) WM–LC periods. Confidence levels at 95% and 99% are indicated by horizontal thin dotted lines. Lag is in months and a negative (positive) lag means that the ENSO leads (lags) the EAWM or NPO.

In summary, our analysis suggests a significant simultaneous triple connection among the EAWM, NPO, and ENSO in the western North Pacific during the SM–HC, which vanishes in the WM–LC, during which the ENSO influence is more preferentially projected onto the PNA-like pattern in the eastern basin. Finally, it is interesting to relate Fig. 11 with Fig. 9 as both show a clear eastward shift of extratropical circulation patterns in the WM–LC compared to the SM–HC, so that the decadal changes of storm-track-associated patterns (Fig. 9) could be partly explained by the ENSO pattern (Fig. 11), although the ENSO index itself does not show any decadal shift around 1988 (Fig. 1).

d. A tentative mechanism for the nonstationarity

The horizontal component of stationary wave activity flux (Plumb 1985) is a useful diagnostic for identifying the source and propagation of anomalous quasi-stationary waves in the middle to upper troposphere (Karoly et al. 1989). To better understand the regime-dependent tropical–extratropical connection in the western North Pacific in terms of stationary wave activity flux, we regressed winter $Z500$ anomalies on the WP index for the SM–HC and WM–LC and calculated the regime-dependent stationary wave activity flux according to the approach of Karoly et al. (1989). A similar analysis but for the NPO for different periods has been previously discussed by Wang et al. (2007). Figure 12 shows the wave activity flux at 500 hPa associated with the WP pattern in the two contrasting periods as well as their difference (SM–HC minus WM–LC). During the SM–HC (Fig. 12a), the WP-regressed anomalous $Z500$ field reveals high-latitude negative anomalies that are widely developed over entire northern Eurasia, from west Russia, passing through Siberia, to the Bering Strait. This widespread negative anomaly field contains two centers: one near the Ural blocking center and the other near the Kamchatka blocking center. Associated with the Ural blocking is the wave activity flux coming from Scandinavia, showing a gradual equatorward bending downstream of the blocking, a feature largely consistent with the wave activity flux associated with the amplification of the Siberian high described in Takaya and Nakamura (2005a).

On the other hand, in the Kamchatka blocking case the incoming poleward wave activity flux propagates northward across the East China Sea and JES, where the flux intensifies substantially and bends progressively northeastward before arriving at the north of Kamchatka. This represents a remarkable poleward wave activity flux originating from the subtropics. Note that the propagation of Rossby waves depends on the basic state and the region of mean westerlies (easterlies) in the extratropical (tropical) western North Pacific is favorable (unfavorable) for their propagation (Dawson et al. 2011). Note also that the amplification of wave activity over the JES is consistent with Yamamoto and Hirose (2011), who suggested a tight dynamic link between the JES cold SST and the enhancement of the Okhotsk low, although such a link is inconclusive in a more recent work by Seo et al. (2014). At midlatitudes, there is a wave train–like anomalous $Z500$ pattern that developed all the way from the central North Pacific to the central North Atlantic, with associated wave activity propagating dominantly eastward between the two oceans across North America.

In contrast, the WP-regressed anomalous $Z500$ field for the WM–LC (Fig. 12b) is mostly confined within the North Pacific basin and eastern Siberia, with associated wave activity flux remarkably weakening by a factor of 2 or more compared to the former period. Also, there is no evidence of the poleward propagation of wave activity along the western margin, nor of the eastward propagation of the midlatitude wave train–like feature between the Pacific and Atlantic basins, in stark contrast to the SM–HC epoch. We suggest, therefore, that the tropical–extratropical teleconnection associated with the WP pattern of anomalous atmospheric circulation can be achieved via the propagation of stationary wave activity along the western margin of the North Pacific,

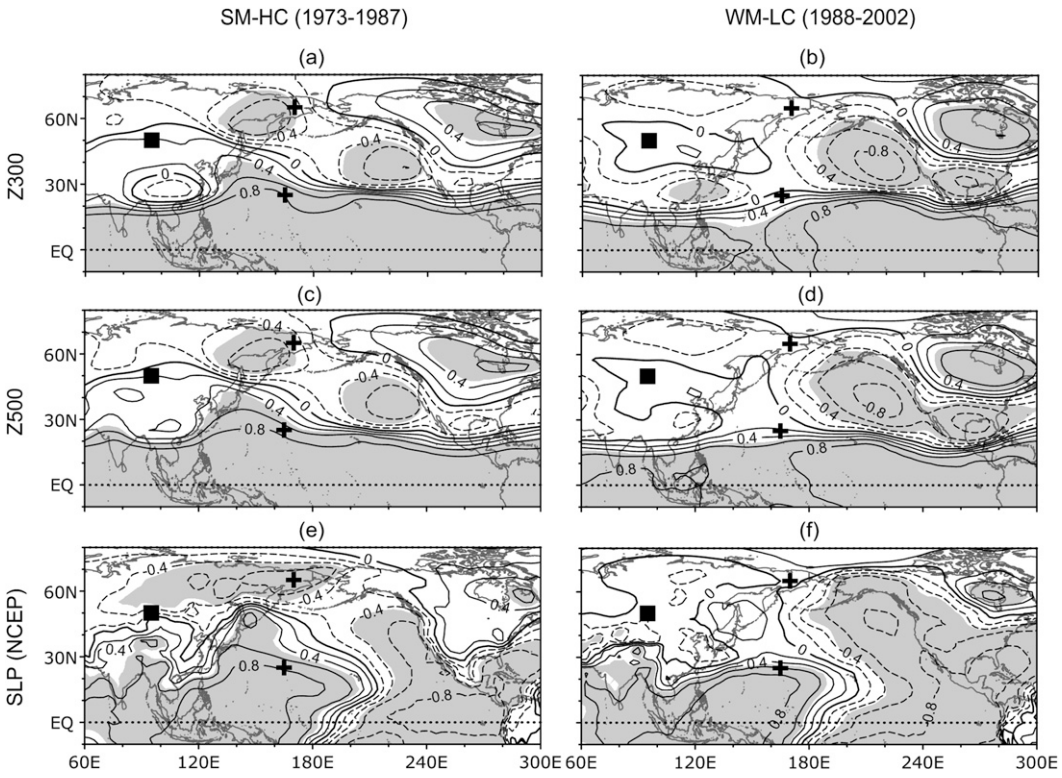

FIG. 11. Maps of correlation of the ENSO index with anomalous winter (DJF) NCEP (a),(b) *Z*300; (c),(d) *Z*500; and (e),(f) SLP for the (left) SM–HC and (right) WM–LC periods. Shading indicates the areas of significant correlation above the 95% level. Centers of action for the SH and NPO are marked by black squares and crosses, respectively.

a mechanism valid for the SM–HC but not for the WM–LC period.

To understand why there is a regime-dependent poleward flux of stationary wave activity in the western margin of the North Pacific we examine in Fig. 13 anomalous SLP, surface winds, and surface air temperature regressed on both the EAWM and negative ENSO indices for the SM–HC and WM–LC as well as their difference (SM–HC minus WM–LC). The negative (positive) ENSO index corresponds to the La Niña (El Niño) phase of ENSO and is used here to compare better, with the influence of the EAWM having generally a simultaneous negative correlation with ENSO (Fig. 10). Although in the extratropics there are interesting features of the NPO-dominant EAWM-related pattern in the western North Pacific during the SM–HC (Fig. 13a as compared to Fig. 13b) and the PNA-dominant ENSO-related pattern in the eastern basin during the WM–LC (Fig. 13e as compared to Fig. 13d), we focus here on the regime-dependent tropical patterns in surface variables because we are mostly interested in tropical heating sources.

The EAWM- and ENSO (La Niña)-related patterns in the tropics south of 20°N during the SM–HC (Figs. 13a,d) are very similar, with both showing a widespread surface air cooling associated with anomalous easterlies over the central and eastern tropical Pacific and anomalous westerlies over the eastern tropical Indian Ocean. In addition, both patterns show an isolated tropical warming in the Philippine Sea, which extends toward the subtropical central North Pacific along with anomalous southwesterlies originating from the equator between 130° and 160°E. There is evidence in both patterns of an anomalous cyclonic circulation centered near the Philippines (10°N, 125°E), with cold northerlies in the South China Sea and warm southerlies in the Philippine Sea. The observed high degree of similarity between the EAWM- and La Niña–related tropical patterns during the SM–HC is consistent with the Pacific–East Asian teleconnection mechanism of Wang et al. (2000), who argued that the anomalous Philippine Sea cyclone (anticyclone) links the central tropical Pacific cooling (warming) and strong (weak) EAWM. Wang et al. (2000) further mentioned that the anomalous Philippine Sea cyclone is associated with enhanced convective heating and promotes anomalous upward motion, inducing upper-level divergence. In contrast, during the WM–LC, both the Philippine Sea cyclone and associated warming

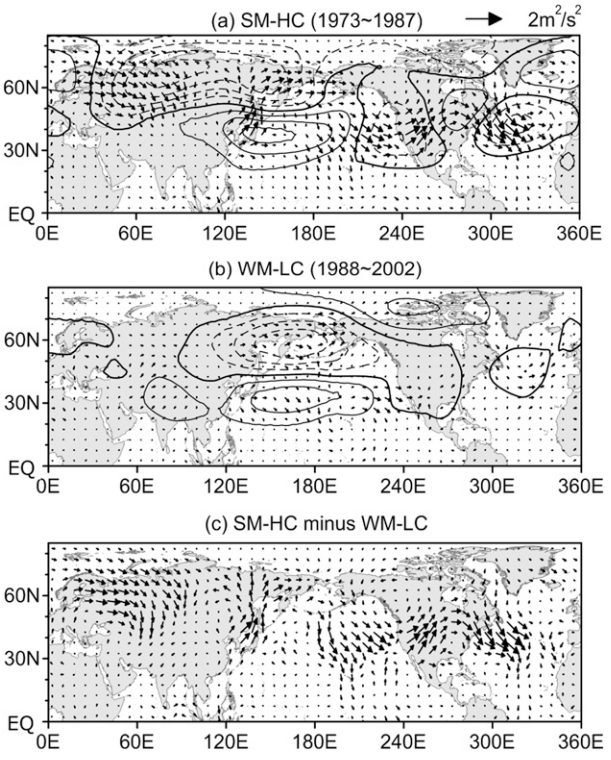

FIG. 12. Stationary wave activity flux (in $m^2 s^{-2}$; scale is given in the top-right corner) superimposed on the anomalous winter $Z500$ field regressed on the WP index for the (a) SM–HC and (b) WM–LC periods. (c) Difference in wave activity flux between the two periods.

disappear in the EAWM pattern (Fig. 13b), while the nearly identical or even slightly enhanced warming compared to the SM–HC is observed in the ENSO pattern (Fig. 13e). This similarity of tropical ENSO pattern for the two periods is consistent with the already-mentioned nonexistence of the 1988 regime shift for ENSO. This information may suggest that the Pacific–East Asian teleconnection mechanism works well for the SM–HC but does not hold for the WM–LC, consistent with the contrasting correlations between the EAWM and ENSO during the two periods (see Table 1).

Finally, we examine the regime-dependent propagation of Rossby waves. Surface heating especially in the tropics drives anomalous convection, which releases latent heat, and the surface precipitation rate is a useful parameter to measure the vertically integrated latent heat release (Dawson et al. 2011). Also, a series of alternating upper-level divergence (associated with convection) and convergence (associated with subsidence) can be generated by a propagating Rossby wave train. However, the surface precipitation rate depends greatly on the weather conditions especially on the presence of cyclones and storms (Trenberth 2011); thus, the vertical motion (convection/subsidence) inferred from it might be much biased by extratropical storm-track activity. Therefore, we instead used the total precipitable water (TPW), which is believed to be less sensitive to storm-track activity, to infer propagating Rossby waves, assuming that a positive (negative) TPW may correspond to an upper-level divergence (convergence) centered at an anomalous anticyclone (cyclone) in the upper-level circulation field. With this idea in mind, we show in Fig. 14 maps of correlation between the TPW at each data point and three climate indices (EAWM, −NPO, and −ENSO) for the SM–HC (Figs. 14a,c,e) and WM–LC (Figs. 14b,d,f). The monthly TPW data we used are from the NCEP–NCAR Reanalysis-1 mentioned in section 2. During the SM–HC, there clearly are three well-defined centers of alternating positive–negative–positive TPW anomalies along the western margin of the North Pacific, each located in the vicinity of the Philippines, the Korean Peninsula, and the Okhotsk Sea. The latter places correspond reasonably well to the theoretical Rossby wave train forced by a western Pacific equatorial heating source placed at 120°E in Jin and Hoskins (1995, their Fig. 16d). We note, however, the tropical–extratropical teleconnection along the western margin is significantly stronger and more widely developed in the EAWM- and NPO-related patterns (Figs. 14a,c), which reveal nearly the same feature, than in the ENSO pattern (Fig. 14e). This might be related to a positive combination or near-resonant interaction (Held et al. 2002) between the tropical heating-induced Rossby wave train and the Tibetan orography-induced anomalous cyclone of the East Asian trough, which should yield stationary waves much stronger than those generated by tropical heating alone.

During the WM–LC, the western margin teleconnection weakens considerably in all three patterns (Figs. 14b,d,f) and there appears to be no complete connection between the tropics and high latitudes, with the interruption occurring in the vicinity of the Korean Peninsula. This interruption is associated with a significant weakening of the East Asian trough during the WM–LC (see Fig. 4b for a pronounced anomalous $Z500$ anticyclone centered at 45°N, 125°E), which combines negatively (or destructively) with the tropical heating-induced wave train, thus inhibiting the latter from propagating farther northward. The clearest example for this may be the ENSO pattern (Fig. 14f) showing no evidence of the northward propagation of the Philippine Sea signal despite a slightly enhanced TPW in the Philippine Sea during the WM–LC, which is rather consistent with a slightly enhanced surface air temperature (Fig. 13e). In addition, the NPO pattern

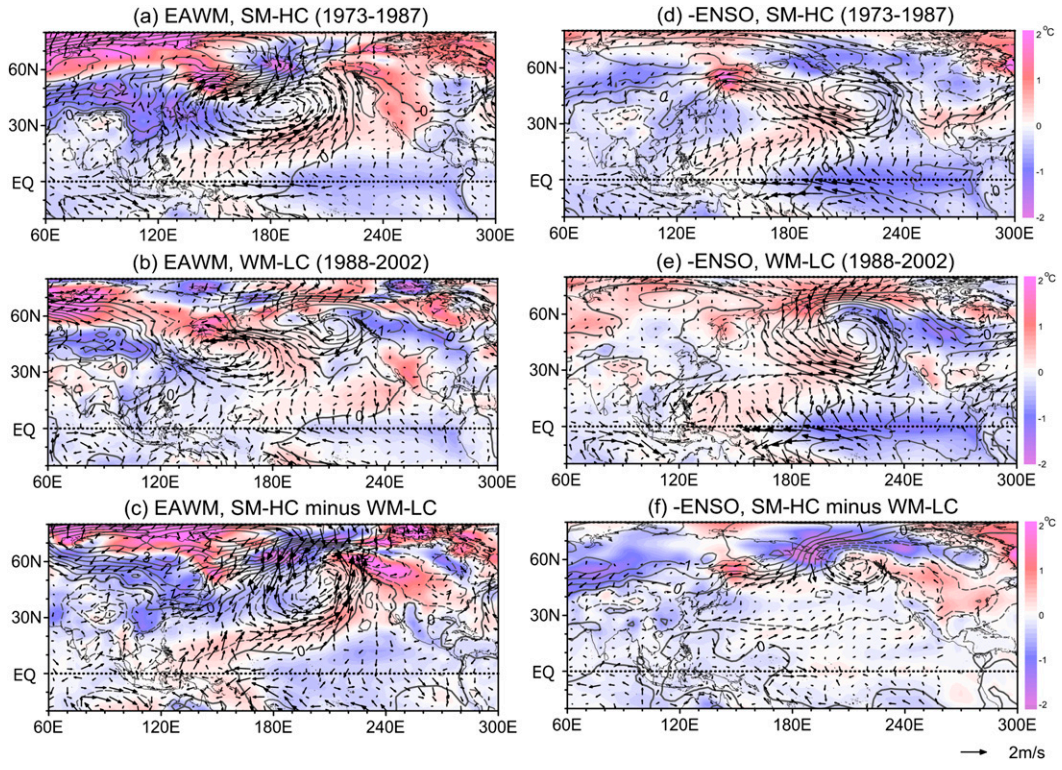

FIG. 13. Regression of anomalous winter surface air temperature (color shading), SLP (contour), and surface winds (arrow) on the EAWM index during the (a) SM–HC and (b) WM–LC periods and (c) their difference. (d)–(f) As in (a)–(c), but on the negative ENSO index. Contour interval for SLP is 0.5 hPa and the scales for temperature and winds are indicated.

during the WM–LC (Fig. 14d) is mostly disconnected from the tropics. On the other hand, there is an eastward shift of the significant Okhotsk signal toward the eastern basin, which is likely related to the eastward shift of the storm-track pattern (Fig. 9), which is in turn partly explained by the eastward intensified ENSO pattern during the WM–LC (Fig. 14f), as mentioned previously.

Based on the above analyses, a tentative mechanism for the nonstationary relationship between the EAWM and NPO is proposed as follows: During the SM–HC, the East Asian trough deepens because of the strengthened Tibetan orographic forcing under strong monsoon winds, creating an anomalous upper-level cyclone north of the Korean Peninsula (Fig. 4b; the sign is to be reversed for the SM–HC anomalies). The latter cyclone is in phase with the Rossby wave train generated by tropical heating in the Philippine Sea (Figs. 11c and 12a), thus reinforcing the latter by a near-resonant effect. This intensified tropical–extratropical teleconnection along the western margin, as clearly evidenced by the northward-propagating significant wave activity flux (Fig. 12), makes a tight triple connection among the EAWM, NPO, and ENSO during the SM–HC. On the other hand, the abrupt decline of the EAWM after the 1988 regime shift induces a concomitant weakening of the East Asian trough, creating a pronounced anomalous anticyclone north of the Korean Peninsula (Fig. 4b), which is in opposite phase with the Rossby wave train originating from the tropics, thus inhibiting the wave train from propagating farther northward. Therefore, the connection between the EAWM and NPO through the tropical teleconnection along the western margin breaks down in the WM–LC. In addition, the eastward shift of the storm track and the associated circulation pattern in the WM–LC (also associated with the tropical teleconnection) may further unfavor the tight connection between EAWM and NPO. Our analysis highlights the pivotal role played by a decadal shift of the East Asian trough, an immediate consequence of the 1988 regime shift of the EAWM. We may conclude therefore that the primary cause of the nonstationary relationship between the EAWM and NPO is the recent abrupt decline of the EAWM since the late 1980s, if one admits the latter decline as a starting point of discussion, although the latter issue is currently the subject of active research as mentioned in section 5a.

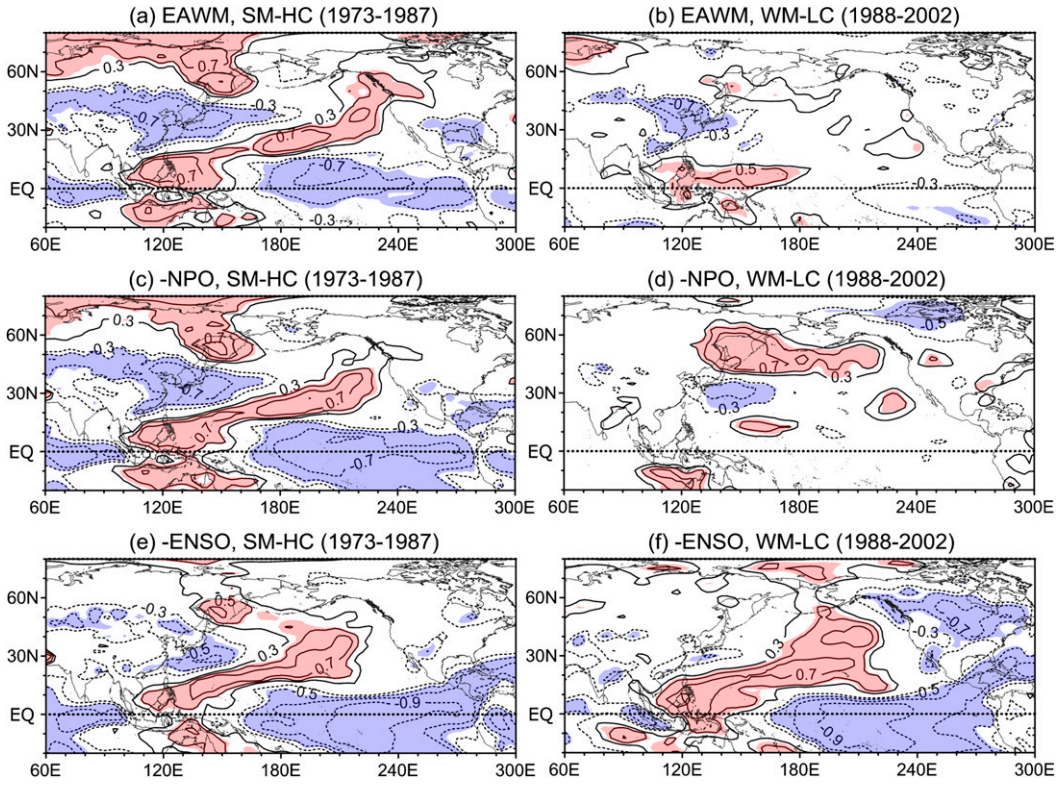

FIG. 14. Maps of correlation between the total precipitable water and the EAWM index for the (a) SM–HC and (b) WM–LC. (c),(d) As in (a),(b), but for the negative NPO index. (e),(f) As in (a),(b), but for the negative ENSO index. Color shading indicates the areas of significant correlation above the 95% level.

6. Summary and discussion

a. The 1988 regime shift and nonstationary relationship between the EAWM and NPO

The EAWM (determined nearly entirely by the SH variability) and the NPO (a surface expression of the WP) form two predominant climate modes affecting the winter climate of the Far East and the western North Pacific. By analyzing data over a total of 48 winter seasons (1965–2012), we have shown that all the above four climate indices underwent an abrupt regime shift around 1988, from a strong winter monsoon regime before 1988 to a weaker monsoon regime afterward. The 11-yr running correlation indicates that the EAWM and NPO were tightly connected to each other during the last two thirds of the strong monsoon regime (1973–87; SM–HC epoch) but nearly completely disconnected during the first two-thirds of the weak monsoon regime (1988–2002; WM–LC epoch).

This regime-dependent nonstationary relationship between the EAWM and NPO is related to a tight (insignificant) statistical connection in SLP variations between the SH and NPO centers of action during the SM–HC (WM–LC) epoch. This is also associated with the pronounced decadal weakening of the SH system over the entire Eurasian continent after the 1988 regime shift as well as the concomitant, positive NPO/WP-like dipole change in surface and upper-level circulation patterns over the North Pacific. It is also shown that the EAWM and NPO are consistently well linked to the upper-level blocking events, Ural and Kamchatka blockings, which explain predominantly the variability of the SH and WP, respectively. This is generally consistent with Takaya and Nakamura (2013).

These leading modes of atmospheric surface circulation variability affect the western North Pacific SST differently in each regime. During the SM–HC, when the EAWM and NPO were strongly connected to each other, a very similar spatial pattern of SST anomalies was projected by these circulation modes, while a quite dissimilar and weakened pattern was observed during the WM–LC when the EAWM and NPO were practically independent. In particular, the EAWM impact on SST during the latter epoch shrank remarkably into a limited area in the East China Sea, making a clear distinction from the NPO impact.

We have paid special attention to the understanding of the dynamics and mechanism underlying the nonstationary relationship between the EAWM and NPO,

a challenging issue not addressed previously. Statistical analyses on the evolution across the 1988 regime shift of storm tracks and tropical influence (ENSO) enabled us to better understand the Northern Hemisphere winter tropical–extratropical teleconnection in the North Pacific, which also reveals a nonstationary decadal evolution: a significant triple connection among the EAWM, NPO, and ENSO in the western North Pacific basin during the SM–HC, which vanishes in the WM–LC when the ENSO influence is more preferentially projected onto the PNA teleconnection pattern in the eastern basin.

In particular, the correlations between the total precipitable water (a measure of the convection/subsidence inherent to a propagating Rossby wave train) and the above three indices (Fig. 14) suggest a tentative mechanism for the nonstationary relationship between the EAWM and NPO as follows: During the SM–HC, the East Asian trough deepens because of the enhanced Tibetan orographic forcing under strengthened monsoon winds, creating a well-developed anomalous upper-level cyclone north of the Korean Peninsula. This anomalous cyclone is in phase with the Rossby wave train generated by tropical heating in the Philippine Sea, which reinforces the latter wave train by a near-resonant effect, yielding a tight triple connection among the EAWM, NPO, and ENSO. On the other hand, the abrupt decline of the EAWM after its 1988 regime shift induces a concomitant weakening of the East Asian trough, yielding a pronounced anomalous anticyclone (as seen north of the Korean Peninsula in Fig. 4b) that is locally out of phase to the Rossby wave train originating from the tropics, thus inhibiting the wave train from propagating farther northward. As a consequence, the triple connection among the EAWM, NPO, and ENSO vanishes. This study highlights the pivotal role played by a decadal shift of the East Asian trough resulting from the 1988 regime shift of the EAWM. We conclude therefore that the nonstationary relationship between the EAWM and NPO is primarily attributable to the recent abrupt decline of the EAWM since the late 1980s, although the causality of the latter decline remains to be investigated.

b. *Concluding remarks*

Our results are consistent with the recent study by Takaya and Nakamura (2013) regarding the tight connection of circulation patterns between the lower- and upper-level troposphere. They showed that enhanced monsoon activity in January is concomitantly associated with the WP-like pattern over eastern Siberia/Alaska and the Eurasian (EU)-like pattern over the Eurasian continent. In our case, the WP-like pattern is strongly connected with the NPO and the EU-like pattern with the EAWM because the latter has been defined as the normalized SLP difference between the two eastern centers of action of the EU pattern: that is, the SH center and the JES center (Park et al. 2012). One important difference is that Takaya and Nakamura (2013), who used their EAWM index for only the period up to 1994 probably because of the availability of the station data they used, consider that the EU-like and WP-like patterns form the two aspects of the same winter monsoon activity. In contrast to this, we treated them here as two separate climate indices (EAWM and NPO), which were highly correlated to each other in the SM–HC epoch (1973–87) but became practically independent in the WM–LC epoch (1988–2002). To resolve this apparent difference in interpretation, a similar analysis as that of Takaya and Nakamura (2013) is warranted to extend up to the most recent years.

One may wonder whether our results are sensitive to the choice of the EAWM index because a number of diverse definitions of the index have been proposed in the literature. The interested reader for this issue is referred to the appendix, where the justification of our EAWM index is given.

It is worth emphasizing that we have considered here only the atmospheric circulation influence on SST variability, deliberately ignoring the ocean dynamics, which may not be always appropriate depending on the period. For example, Park et al. (2012) showed that in the period 1970–89 the EAWM was largely responsible for the SST variability in most of the western North Pacific, whereas ocean dynamics became increasingly important there over the period 1990–2005. If this is true, the impact of ocean dynamics on SST should be included in the analysis of the atmosphere–ocean interaction in the western North Pacific, especially during the WM–LC epoch, which is a separate effort undergoing presently.

Finally, our results solely based on statistical analyses cannot provide the full details regarding two-way atmosphere–ocean interactions and are inherently limited in attributing the exact cause of the regime shift around 1988. This should be the scope of dedicated numerical experiments, which are left for future work.

Acknowledgments. This paper has been prepared as part of the dual doctoral cooperation between the University of Paris VI and Seoul National University (SNU). G. Pak has been supported from the Brain Korea 21 Project of SNU, for which we are very grateful to K.-R. Kim, and also from the Ministry of Oceans and Fisheries, South Korea (OCCAPA and EAST-I projects). Y.-O. Kwon is supported by the U.S. National Science Foundation Climate and Large-Scale Dynamics program (AGS-1035423) and Department of Energy (DOE)

Climate and Environmental Science Division (DE-SC0007052). We enjoyed insightful discussion with B.-M. Kim on the synoptic eddy feedback on low-frequency flow. The original manuscript has been significantly strengthened thanks to three anonymous reviewers.

APPENDIX

Justification of Our EAWM Index

Wang and Chen (2010) classified 18 existing indices into four categories according to the definition of the monsoon strength using different parameters, such as the east–west SLP gradient, low-level meridional winds, upper-level zonal wind shear, and East Asian trough for the 1957–2001 period. These authors assessed the spatial performance of these indices for representing the monsoon-related circulation, precipitation, and lower-tropospheric air temperature anomalies as well as their predictability based on knowledge of ENSO and AO. We remark that most of indices based on low-level meridional winds have been defined for the regions composing the tropics and subtropics (10°–30°N) over East Asia and the western North Pacific (110°–140°E), showing a high correlation (order 0.65) with the ENSO index (see Table 1 of Wang and Chen 2010). On the other hand, the SLP gradient-based indices have been defined mostly for the regions centered at midlatitudes (20°–60°N) using the SLP difference between the eastern lobe of the SH system (110°E) and the western lobe of the AL system (160°E). These latter indices show a moderate correlation (order 0.4) with the ENSO index. A recent paper (Wang and Chen 2014b) suggests that, in addition to the east–west pressure gradient, the north–south pressure gradient between midlatitudes and equatorial region is also important for the winter monsoon. Correspondingly, an index was defined to reflect this feature and good results were obtained.

Because we are interested here in the regime-dependent nonstationary relationship of the EAWM and NPO as well as their connection to the tropical influence, the optimal EAWM index should be the one that shows in climatology the weakest relationship with ENSO but at the same time the strongest correlation with surface climate variables over the midlatitude western boundary region, where the winter monsoon northerlies prevail. In this sense, Park et al. (2012) compared several frequently cited winter monsoon indices with observations-derived surface variables (air temperature, SST, and wind speeds) in the midlatitude East Asian marginal seas region. They concluded that their new EAWM index (defined as the normalized DJF SLP difference between the area-mean SLP over the Siberian center and that near the JES center) that is used in the present study reveals the best performance in explaining the variability of winter surface variables of the region from selected station data. This index, $EAWM_{Park}$, reveals the practically same performance as the SH index, an indisputable index for gauging the winter monsoon strength over East Asia (Gong et al. 2001), which shows the weakest relationship with (thus most independent from) ENSO and AO (see Table 1). Figure A1 shows that $EAWM_{Park}$ correlates remarkably well ($r = 0.83$) with a recent EAWM index proposed by Takaya and Nakamura (2013), $EAWM_{Takaya}$, which is defined as normalized winter surface air temperature anomalies averaged over the midlatitude Far East and marginal seas region (25°–40°N, 100°–140°E). However, these surface air temperature anomalies show only a marginal correlation ($r = 0.35$) with 850-hPa meridional wind anomalies over the region, corresponding to the index proposed by Yang et al. (2002) ($EAWM_{Yang}$). We have deliberately refrained from testing other EAWM indices defined in regions composing the tropics because of their inevitable "contamination" by strong ENSO signals (see Fig. 11).

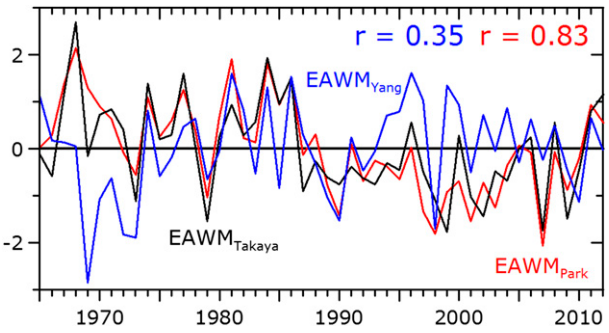

FIG. A1. Comparison of $EAWM_{Park}$ (red) and $EAWM_{Yang}$ (blue) in reference to $EAWM_{Takaya}$ (black), with corresponding correlation coefficients given ($EAWM_{Park}$: $EAWM_{Takaya} = 0.83$; $EAWM_{Yang}$: $EAWM_{Takaya} = 0.35$).

REFERENCES

Barriopedro, D., R. Garcia-Herrera, A. R. Lupo, and E. Hernandez, 2006: A climatology of Northern Hemisphere blocking. *J. Climate,* **19,** 1042–1063, doi:10.1175/JCLI3678.1.

Ceballos, L. I., E. Di Lorenzo, C. D. Hoyos, N. Schneider, and B. Taguchi, 2009: North Pacific Gyre Oscillation synchronizes climate fluctuations in the eastern and western boundary systems. *J. Climate,* **22,** 5163–5174, doi:10.1175/2009JCLI2848.1.

Chang, C. P., M. M. Lu, and B. Wang, 2011: The East Asian winter monsoon. *The Global Monsoon System: Research and Forecast,* 2nd ed., C. P. Chang et al., Eds., World Scientific, 99–109.

Dawson, A., A. J. Matthews, and D. P. Stevens, 2011: Rossby wave dynamics of the North Pacific extra-tropical response to El Niño: Importance of the basic state in coupled GCMs. *Climate Dyn.,* **37,** 391–405, doi:10.1007/s00382-010-0854-7.

Emery, W. J., and R. E. Thomson, 1997: *Data Analysis Methods in Physical Oceanography*. Pergamon, 638 pp.

Frankignoul, C., N. Sennechael, Y.-O. Kwon, and M. A. Alexander, 2011: Influence of the meridional shifts of the Kuroshio and the Oyashio Extensions on the atmospheric circulation. *J. Climate,* **24,** 762–777, doi:10.1175/2010JCLI3731.1.

Gong, D.-Y., S.-W. Wang, and J.-H. Zhu, 2001: East Asian winter monsoon and Arctic Oscillation. *Geophys. Res. Lett.,* **28,** 2073–2076, doi:10.1029/2000GL012311.

Hare, S. R., and N. J. Mantua, 2000: Empirical evidence for North Pacific regime shifts in 1977 and 1989. *Prog. Oceanogr.,* **47,** 103–145, doi:10.1016/S0079-6611(00)00033-1.

Held, I. M., and M. Ting, 1990: Orographic versus thermal forcing of stationary waves: The importance of the mean low-level wind. *J. Atmos. Sci.,* **47,** 495–500, doi:10.1175/1520-0469(1990)047<0495:OVTFOS>2.0.CO;2.

——, ——, and H. Wang, 2002: Northern winter stationary waves: Theory and modeling. *J. Climate,* **15,** 2125–2144, doi:10.1175/1520-0442(2002)015<2125:NWSWTA>2.0.CO;2.

Hirose, N., K. Nishimura, and M. Yamamoto, 2009: Observational evidence of a warm ocean current preceding a winter teleconnection pattern in the northwestern Pacific. *Geophys. Res. Lett.,* **36,** L09705, doi:10.1029/2009GL037448.

Hori, M. E., and H. Ueda, 2006: Impact of global warming on the eastern Asian winter monsoon as revealed by nine coupled atmosphere–ocean GCMs. *Geophys. Res. Lett.,* **33,** L03713, doi:10.1029/2005GL024961.

Huang, R., J. Chen, L. Wang, and Z. Lin, 2012: Characteristics, processes and causes of the spatio-temporal variabilities of the East Asian monsoon system. *Adv. Atmos. Sci.,* **29,** 910–942, doi:10.1007/s00376-012-2015-x.

Jin, F.-F., and B. J. Hoskins, 1995: The direct response to tropical heating in a baroclinic atmosphere. *J. Atmos. Sci.,* **52,** 307–319, doi:10.1175/1520-0469(1995)052<0307:TDRTTH>2.0.CO;2.

Kalnay, E., and Coauthors, 1996: The NCEP/NCAR 40-Year Reanalysis Project. *Bull. Amer. Meteor. Soc.,* **77,** 437–471, doi:10.1175/1520-0477(1996)077<0437:TNYRP>2.0.CO;2.

Karoly, D. J., R. A. Plumb, and M. Tang, 1989: Examples of the horizontal propagation of quasi-stationary waves. *J. Atmos. Sci.,* **46,** 2802–2811, doi:10.1175/1520-0469(1989)046<2802:EOTHPO>2.0.CO;2.

Kwon, Y.-O., M. A. Alexander, N. A. Bond, C. Farnkignoul, H. Nakamura, B. Qiu, and L. A. Thompson, 2010: Role of the Gulf Stream and Kuroshio–Oyashio systems in large-scale atmosphere–ocean interaction: A review. *J. Climate,* **23,** 3249–3281, doi:10.1175/2010JCLI3343.1.

Li, F., H. Wang, and Y. Gao, 2014: On the strengthened relationship between the East Asian winter monsoon and Artic Oscillation: A comparison of 1950–70 and 1983–2012. *J. Climate,* **27,** 5075–5091, doi:10.1175/JCLI-D-13-00335.1.

Linkin, M. E., and S. Nigam, 2008: The North Pacific Oscillation–west Pacific teleconnection pattern: Mature-phase structure and winter impacts. *J. Climate,* **21,** 1979–1997, doi:10.1175/2007JCLI2048.1.

Nakamura, H., T. Izumi, and T. Sampe, 2002: Interannual and decadal modulations recently observed in the Pacific storm track activity and East Asian winter monsoon. *J. Climate,* **15,** 1855–1874, doi:10.1175/1520-0442(2002)015<1855:IADMRO>2.0.CO;2.

Panagiotopoulos, F., M. Shahgedanova, A. Hannachi, and D. B. Stephenson, 2005: Observed trends and teleconnections of the Siberian high: A recently declining center of action. *J. Climate,* **18,** 1411–1422, doi:10.1175/JCLI3352.1.

Park, Y.-H., J.-H. Yoon, Y.-H. Youn, and F. Vivier, 2012: Recent warming in the western North Pacific in relation to rapid changes in the atmospheric circulation of the Siberian high and Aleutian low systems. *J. Climate,* **25,** 3476–3493, doi:10.1175/2011JCLI4142.1.

Plumb, R. A., 1985: On the three-dimensional propagation of stationary waves. *J. Atmos. Sci.,* **42,** 217–229, doi:10.1175/1520-0469(1985)042<0217:OTTDPO>2.0.CO;2.

Rayner, N. A., D. E. Parker, E. B. Horton, C. K. Folland, L. V. Alexander, D. P. Rowell, E. C. Kent, and A. Kaplan, 2003: Global analyses of sea surface temperature, sea ice, and night marine air temperature since the late nineteenth century. *J. Geophys. Res.,* **108,** 4407, doi:10.1029/2002JD002670.

Rodionov, S. N., 2004: A sequential algorithm for testing climate regime shifts. *Geophys. Res. Lett.,* **31,** L09204, doi:10.1029/2004GL019448.

Seo, H., Y.-O. Kwon, and J.-J. Park, 2014: On the effect of the East/Japan Sea SST variability on the North Pacific atmospheric circulation in a regional climate model. *J. Geophys. Res.,* **119,** 418–444, doi:10.1002/2013JD020523.

Takaya, K., and H. Nakamura, 2005a: Mechanisms of intraseasonal amplification of the cold Siberian high. *J. Atmos. Sci.,* **62,** 4423–4440, doi:10.1175/JAS3629.1.

——, and ——, 2005b: Geographical dependence of upper-level blocking formation associated with intraseasonal amplification of the Siberian high. *J. Atmos. Sci.,* **62,** 4441–4449, doi:10.1175/JAS3628.1.

——, and ——, 2013: Interannual variability of the East Asian winter monsoon and related modulations of the planetary waves. *J. Climate,* **26,** 9445–9461, doi:10.1175/JCLI-D-12-00842.1.

Tian, Y., H. Kidokoro, T. Watanabe, and N. Iguchi, 2008: The late 1980s regime shift in the ecosystem of Tsushima warm current in the Japan/East Sea: Evidence from historical data and possible mechanisms. *Prog. Oceanogr.,* **77,** 127–145, doi:10.1016/j.pocean.2008.03.007.

Trenberth, K. E., 2011: Changes in precipitation with climate change. *Climate Res.,* **47,** 123–138, doi:10.3354/cr00953.

——, and D. A. Paolino, 1980: The Northern Hemisphere sea level pressure data set: Trends, errors, and discontinuities. *Mon. Wea. Rev.,* **108,** 855–872, doi:10.1175/1520-0493(1980)108<0855:TNHSLP>2.0.CO;2.

——, and J. W. Hurrell, 1994: Decadal atmosphere–ocean variation in the Pacific. *Climate Dyn.,* **9,** 303–319, doi:10.1007/BF00204745.

Vimont, D. J., J. M. Wallace, and D. S. Battisti, 2003: The seasonal footprinting mechanism in the Pacific: Implications for ENSO. *J. Climate,* **16,** 2668–2675, doi:10.1175/1520-0442(2003)016<2668:TSFMIT>2.0.CO;2.

Wallace, J. M., and D. S. Gutzler, 1981: Teleconnections in the geopotential height field during the Northern Hemisphere winter. *Mon. Wea. Rev.,* **109,** 784–812, doi:10.1175/1520-0493(1981)109<0784:TITGHF>2.0.CO;2.

Wang, B., R. Wu, and X. Fu, 2000: Pacific–East Asian teleconnection: How does ENSO affect East Asian climate? *J. Climate,* **13,** 1517–1536, doi:10.1175/1520-0442(2000)013<1517:PEATHD>2.0.CO;2.

Wang, L., and W. Chen, 2010: How well do existing indices measure the strength of the East Asian winter monsoon? *Adv. Atmos. Sci.,* **27,** 855–870, doi:10.1007/s00376-009-9094-3.

——, and ——, 2014a: The East Asian winter monsoon: Re-amplification in the mid-2000s. *Chin. Sci. Bull.,* **59,** 430–436, doi:10.1007/s11434-013-0029-0.

——, and ——, 2014b: An intensity index for the East Asian winter monsoon. *J. Climate,* **27,** 2361–2374, doi:10.1175/JCLI-D-13-00086.1.

——, ——, and R. Huang, 2007: Changes in the variability of North Pacific Oscillation around 1975/1976 and its relationship with East Asian winter climate. *J. Geophys. Res.,* **112,** D11110, doi:10.1029/2006JD008054.

——, R. Huang, L. Gu, W. Chen, and L. Kang, 2009: Interdecadal variations of the East Asian winter monsoon and their association with quasi-stationary planetary wave activity. *J. Climate,* **22,** 4860–4872, doi:10.1175/2009JCLI2973.1.

——, W. Chen, W. Zhou, J. C. J. Chan, D. Barriopedro, and R. Huang, 2010: Effect of the climate shift around mid 1970s on the relationship between wintertime Ural blocking circulation and East Asian climate. *Int. J. Climatol.,* **30,** 153–158, doi:10.1002/joc.1876.

Yamamoto, M., and N. Hirose, 2011: Possible modification of atmospheric circulation over the northwestern Pacific induced by a small semi-enclosed ocean. *Geophys. Res. Lett.,* **38,** L03804, doi:10.1029/2011GL047134.

Yang, S., K. Lau, and K. Kim, 2002: Variations of the East Asian jet stream and Asian–Pacific–American winter climate anomalies. *J. Climate,* **15,** 306–325, doi:10.1175/1520-0442(2002)015<0306:VOTEAJ>2.0.CO;2.

Yeh, S.-W., and C.-H. Kim, 2010: Recent warming in the Yellow/East China Sea during winter and the associated atmospheric circulation. *Cont. Shelf Res.,* **30,** 1428–1434, doi:10.1016/j.csr.2010.05.002.

——, Y.-J. Kang, Y. Noh, and A. J. Miller, 2011: The North Pacific climate transitions of the winters of 1976/77 and 1988/89. *J. Climate,* **24,** 1170–1183, doi:10.1175/2010JCLI3325.1.

Zhu, W., and Z. Sun, 1999: Influence of ENSO event on the maintenance of Pacific storm track in the northern winter. *Adv. Atmos. Sci.,* **16,** 630–640, doi:10.1007/s00376-999-0037-9.